J. Chil. Chem. Soc., 69, N°3 (2024)

SYNTHESIS, ELECTRONIC AND PHOTOPHYSICAL PROPERTIES OF 3,8-DIAROMATIC-1,10-PHENANTHROLINE MOLECULES

JOSÉ MUÑOZ[1], FELIPE PEÑALOZA [1], KEVIN GUAJARDO [1], ROXANA ARCE [1,2], NANCY PIZARRO [1] AND ANDRÉS VEGA [1,3]*

[1]Universidad Andres Bello, Facultad de Ciencias Exactas, Departamento de Ciencias Químicas.
[2]Millennium Institute on Green Ammonia as Energy Vector - MIGA (ICN2021_023).
[3]Centro para el Desarrollo de la Nanociencia y la Nanotecnología, CEDENNA.

ABSTRACT

The molecules 3,8-diphenyl-1,10-phenanthroline (**L$_1$**), 3,8-di(naphthalen-1-yl)-1,10-phenanthroline (**L$_2$**), 3,8-di(naphthalen-2-yl)-1,10-phenanthroline (**L$_3$**), 3,8-di(anthracen-9-yl)-1,10-phenanthroline (**L$_4$**), and 3,8-di(pyren-1-yl)-1,10-phenanthroline (**L$_5$**) were prepared in good yield from the reaction of 3,8-dibromo-1,10-phenanthroline with the corresponding boronic acid, catalysed by [Pd(PPh$_3$)$_4$]. Computational DFT modelling suggests that the aromatic substituent arms are not coplanar with the central phenanthroline (*phen*) core, and that the HOMO-LUMO gap diminishes as the number of fused carbon rings in the arms increases. Cyclic voltammograms for the ligands show between one and two oxidation and one to three reduction waves, which are believed to be centred on the arms and the central *phen* fragments, respectively, suggesting some small electronic mixing. The absorption and emission properties depend on the electronic interaction between the polyaromatic substituents and the phenanthroline core. Different emissive ππ* excited states for the molecules bearing anthryl and pyrenyl substituents suggest they have more charge transfer character, and a consequent sensitivity to the increase of solvent polarity. The photosensitizing capacity of singlet oxygen generation upon excitation of **L$_1$**-**L$_5$** in solution is consistent with a significant evolution of the former singlet excited state towards a triplet excited state.

Keywords: 1,10-phenanthroline, photophysical, voltammetry, 3,8-diaromatic.

INTRODUCTION

In the recent years, polypyridine ligands have stood out due to their great versatility in different fields of knowledge, especially in coordination chemistry applications [1]. This type of ligands have the ability to bind to different metals ions, such as rhenium(I), ruthenium(II), iridium(III) or copper(II) to form stable complexes with remarkable properties, such as luminescence, for biological applications [2], photodynamic therapy for the treatment of cancer [3], development of energy capture systems through sensitizers in dye-sensitized solar cells [4], applications in electronic molecule through design of OLEDs components [5] and metallopharmaceuticals and materials science [6]. In this sense, efforts have also been concentrated on the development of complexes with polypyridyl ligands for applications in photochemistry, photophysics, photocatalysis, electrochemistry, photoelectrochemistry and electron and energy transfer [7-10].

1,10-phenanthroline (often abbreviated as *phen*) is a bidentate and chelating rigid aromatic molecule widely used as ligand to prepare metal complexes for many diverse uses [11, 12]. Derivatization of the *phen* core opens up new possibilities and applications for these new molecules [13], particularly as ligands [14-18]. 3,8-diphenyl-1,10-phenanthroline (referred as **L$_1$** as shown Scheme 1) was first synthesized in the mid-1950s by reacting phenylenediamine with ethyl α,α-formylphenyl-acetate, followed by reduction with hydrogen [19]. Recent reports suggest that it can also be prepared from direct arylation [20]. Despite the pronounced effects of phenyl substituents on the photophysical properties of rhenium(I) tricarbonyl [21] and ruthenium(II) complexes [22], examples of incorporating polyaromatic moieties onto the *phen* core are limited to compounds such as bis(2-(1,1'-binaphthalen-2-yl)-3,8-diphenyl-1,10-phenanthroline) [23] and bis(2-(2-pyridyl)phenyl-C,N)-(3,8-bis(9,9-di-n-hexyl-9*H*-fluoren-2-yl)-1,10-phenanthroline [24].

In this manuscript we describe the syntheses of a series of 3,8-diaromatic-1,10-phenanthroline molecules (L$_1$ – L$_5$ as shown in Scheme 1) with 1 to 4 fused carbon rings. These molecules were obtained by coupling 3,8-dibromo-1,10-phenanthroline with the corresponding boronic acids in the presence of [Pd(PPh$_3$)$_4$]. The photophysical and voltammetric properties are discussed in detail within the context of molecular and electronic structure as determined by DFT modelling.

2. EXPERIMENTAL

Dichloromethane (DCM), 1,4-Dioxane, Ethanol (EtOH), Methanol (MeOH), Acetonitrile (MeCN) of spectroscopic grade, Uvasol® Merck, and chloroform (CHCl$_3$) Seccosolv®Merck, were employed as received. Reactants were also used as obtained from the suppliers: 3,8-Dibromo-1,10-phenanthroline (95%), Phenylboronic acid (98%), 2-Naphthaleneboronic acid (98%), 1-Naphthaleneboronic acid (98%), 9-Anthracenylboronic acid (98%), 1-Pyrenylboronic acid (98%) and 2-Anthraceneboronic acid (98%) were purchased from AkSci. Potassium carbonate and tetrakis(triphenylphosphine)palladium(0) (99%) was obtained from Sigma-Aldrich

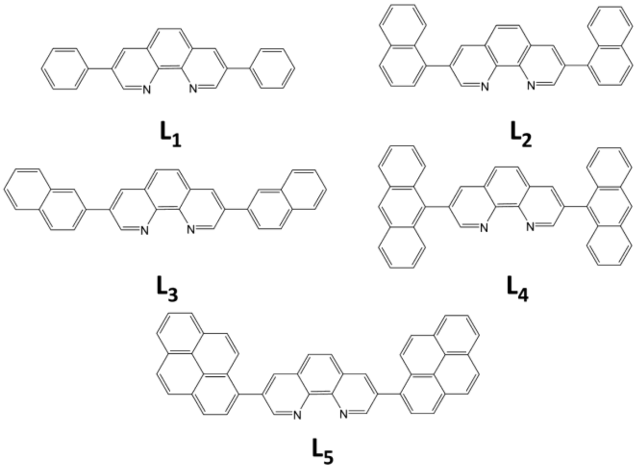

Scheme 1. Diagram for the structure of **L$_1$** to **L$_5$**.

2.1.- Syntheses

2.1.1.- 3,8-diphenyl-1,10-phenanthroline (L$_1$): 1.00 g (8.20 mmol) of phenylboronic acid, 1.10 g 3,8-Dibromo-1,10-phenanthroline (3.28mmol) and 0.100 g of tetrakistriphenylphosphinepalladium(0) [Pd(PPh$_3$)$_4$] were mixed in 50 mL of 1,4-dioxane with stirring and under an argon atmosphere, following what depicted in Scheme 2. 3 mL of 2.0 mol/dm^3 water solution of potassium carbonate were added to the mix, which was then refluxed and stirred for 48 hours, monitored by means of thin layer chromatography. After cooling and solvent removal under reduced pressure, a crude solid product was obtained. This crude product was purified by silica column chromatography using dichloromethane-triethylamine (0.5%) as the eluent. Following fraction collection and solvent evaporation, a colorless powder solid was obtained with a 58.7 % yield. The compound crystallized from a chloroform solution. Single crystal X-ray diffraction shows an orthorhombic cell (*a* = 11.5331(17) Å; *b* = 7.1243(11) Å; *c* = 22.501(4) Å, Space group *Pnma*), although r-factor

---

*Corresponding author email: andresvega@unab.cl remains high despite efforts (approximately 20%). The structure shows the phenyl arms are twisted by 40.0° with respect to the central *phen* core, but they are disordered over two positions as requested by the mirror plane on the symmetry space group (see Figure S15).

MH$^+$: 333.1397 Da. ^{1}HNMR (400 MHz, CDCl3) δ 9.51 (d, J = 1.6 Hz, 1H), 8.47 (d, J = 1.9 Hz, 1H), 7.93 (s, 1H), 7.84 – 7.77 (m, 2H), 7.58 (t, J = 7.5 Hz, 2H), 7.49 (t, J = 7.4 Hz, 1H). ^{13}C NMR (101 MHz, $CDCl_3$) δ 149.51, 145.07, 137.54, 135.70, 133.34, 129.21, 128.44, 128.35, 127.53, 127.07. IR: ῡ = 3413, 1656, 1619, 1426, 1075, 908, 767, 703 cm^{-1}.

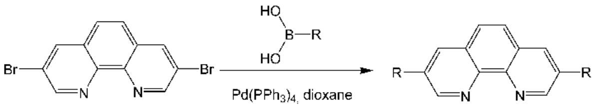

Scheme 2. General synthetic route to $\mathbf{L_1}$ to $\mathbf{L_5}$.

2.1.2.- 3,8-di(naphthalen-1-yl)-1,10-phenanthroline ($\mathbf{L_2}$): A similar procedure to those previously described for $\mathbf{L_1}$. 72% yield. MH$^+$: 433.1712 Da. ^{1}HNMR (400 MHz, CDCl3) δ 9.39 (d, J = 2.2 Hz, 1H), 8.43 (d, J = 2.2 Hz, 1H), 7.99 (dd, J = 11.0, 3.5 Hz, 2H), 7.97 – 7.91 (m, 2H), 7.68 – 7.60 (m, 2H), 7.60 – 7.47 (m, 2H). ^{13}C NMR (101 MHz, $CDCl_3$) δ 151.78, 145.11, 136.48, 136.04, 135.79, 133.83, 131.57, 128.79, 128.54, 128.32, 127.91, 127.04, 126.75, 126.19, 125.45, 125.26. IR ῡ: 3034, 1423, 1367, 916, 803, 780, 728 cm^{-1}.

2.1.3.- 3,8-di(naphthalen-2-yl)-1,10-phenanthroline ($\mathbf{L_3}$): A similar procedure to those previously described for $\mathbf{L_1}$. 85 % yield. MH$^+$: 433.1706 Da. ^{1}H NMR (300 MHz, CDCl3) δ 9.61 (d, J = 2.2 Hz, 1H), 8.58 (d, J = 2.3 Hz, 1H), 8.29 (s, 1H), 8.05 (dd, J = 11.9, 8.9 Hz, 2H), 7.96 (d, J = 10.4 Hz, 3H), 7.67 – 7.53 (m, 2H). ^{13}C NMR (75 MHz, $CDCl_3$) δ 149.78, 145.13, 135.76, 134.87, 133.72, 133.68, 133.04, 129.14, 128.64, 128.41, 127.81, 127.26, 126.78, 126.73, 126.69, 125.29. IR ῡ: 3034, 1630, 1588, 1424, 1361, 1279, 1127, 860, 813, 755 cm^{-1}.

2.1.4.- 3,8-di(anthracen-9-yl)-1,10-phenanthroline ($\mathbf{L_4}$): A similar procedure to those previously described for $\mathbf{L_1}$. 68 % yield. MH$^+$: 533.2001 Da. ^{1}HNMR: (400 MHz, CDCl3) δ 9.35 (d, J = 1.9 Hz, 1H), 8.65 (s, 1H), 8.47 (d, J = 1.8 Hz, 1H), 8.14 (d, J = 8.5 Hz, 2H), 8.01 (s, 1H), 7.71 (d, J = 8.8 Hz, 2H), 7.60 – 7.50 (m, 2H), 7.50 – 7.33 (m, 2H). IR ῡ = 3024, 1746, 1403, 1357, 1220, 883, 785, 728, 632 cm^{-1}.

2.1.5.- 3,8-di(pyren-1-yl)-1,10-phenanthroline ($\mathbf{L_5}$): A similar procedure to those previously described for $\mathbf{L_1}$. 89 % yield. MH$^+$: 581. 2004 Da. ^{1}HNMR: (400 MHz, CDCl3) δ 9.57 (d, J = 2.1 Hz, 1H), 8.60 (d, J = 2.1 Hz, 1H), 8.36 (d, J = 7.8 Hz, 1H), 8.29 – 8.22 (m, 3H), 8.20 – 8.16 (m, 3H), 8.14 (d, J = 9.3 Hz, 1H), 8.09 (d, J = 7.6 Hz, 1H), 8.05 (d, J = 4.3 Hz, 1H). IR ῡ =3034, 1599, 1486, 1424, 1187, 919, 844, 718, 679 cm^{-1}.

2.2.- Spectroscopic and Photophysical Measurements: Measurements were conducted as follows: Infrared spectra (in the range 4000-400 cm^{-1}) were obtained using a Jasco FTIR-4600 spectrophotometer equipped with an ATR PRO ONE. ^{1}H-NMR spectra were recorded on a Bruker Avance 400 MHz spectrometer at 298 K, using $CDCl_3$ as the solvent. Mass spectra were recorder in a high-resolution mass spectrometer (HRMS), Bruker compact TOF, by direct injection and using positive ionization. UV-Vis spectra were captured on an Agilent 8453 Diode-Array spectrophotometer in the range of 250-700 nm using aerated solvent solutions at room temperature. Emission spectra were measured using a Horiba Jobin-Yvon FluoroMax-4 spectrofluorometer in different solvents at room temperature or in ethanol-methanol glass (4:1, v/v) at 77 K. Luminescence lifetime measurements were performed using the time-correlated single photon counting technique with a PicoQuant FluoTime300 fluorescence lifetime spectrometer. A sub-nanosecond pulsed laser at 405 nm served as the light source (FWHM ~ 500 ps, average power 2 mW). Time-resolved experiments were conducted in solution under either air-equilibrated or argon-saturated conditions (solutions were degassed by bubbling argon gas through them for 30 minutes). Emission quantum yields (F_{em}) were determined using procedures described in the literature, employing $[Ru(bpy)_3](PF_6)_2$ in acetonitrile solution as the actinometer [25, 26]. Briefly, the optical densities of the sample (OD_S) and actinometer (OD_{ACT}) solutions were set below 0.10 and matched at the excitation wavelength. The emission quantum yield of each compound was calculated by using Eq. 1[27]:

$$\Phi_S = \Phi_{ACT} x \left(\frac{I_S}{I_{ACT}}\right) x \left(\frac{OD_{ACT}}{OD_S}\right) x \left(\frac{\eta_S}{\eta_{ACT}}\right)^2 \qquad \text{Eq.1}$$

where F_{ACT} is the known quantum yield of the actinometer, I_S and I_{ACT} are the integrated area of the emission spectrum of the sample and actinometer, and h_S and h_{ACT} are the refractive index of sample and actinometer solvent solutions.

Singlet oxygen ($O_2(^1\Delta g)$) emission measurements were carried out using the FluoTime300. For detection at 1270 nm, a near-infrared PMT H10330A (Hamamatsu) was employed. The $O_2(^1\Delta_g)$ quantum yields (F_Δ) were determined by comparing the intensity at zero time of the 1270 nm signals generated by the compounds upon irradiation to those of optically matched solutions of phenalenone as reference [28]. Experiments were repeated at least three times to obtain average values with error less than 10%.

2.3 Cyclic Voltammetry. For the electrochemical experiments, the solution contained 2.0×10^{-3} mol dm^{-3} of each molecule with 1.0×10^{-1} mol dm^{-3} of tetrabutylammonium hexafluorophosphate ($TBAPF_6$) as the supporting electrolyte in dimethylformamide (DMF). Prior to each experiment, the solution was purged with high-purity argon, and an argon atmosphere was maintained over the solution throughout to experience. Additionally, before each measurement the open circuit potential (resting potential) was measured. A fluorine-doped tin oxide (FTO) substrate served as working electrode, while a platinum electrode acted as auxiliary electrode. All potentials quoted in this text refer to an Ag|AgCl electrode at room temperature. The electrochemical experiments were conducted at room temperature using a CHI600E bipotentiostat interfaced with a PC running the CHI software which facilitated experimental control and data acquisition.

2.4.- Computational Details: Geometry optimizations were performed at the B3LYP/6-31+G(d,p) level of theory using the Gaussian16 package of programs (G16) [29]. Crystallographic coordinates served as input for these optimizations when available. Excited state calculations were performed within the time-dependent density functional theory (TD-DFT) methodology, as implemented in G16. When solvent effects were considered, they were incorporated using the polarizable continuum model (PCM) using the integral equation formalism variant (IEFPCM) [30, 31]. Absorption and emission spectra were simulated based on the above calculations using the GaussSum 3.0 suite of freely available processing tools. A full width at half-maximum (FWHM) of the Gaussian curves corresponding to 2500 cm^{-1} was employed to convolute both spectra. Representations for Kohn-Sham orbitals were generated using the Gaussian cubegen tool and have been visualized using VMD and Povray 3.6 programs [32, 33].

3. RESULTS AND DISCUSSION

3.1.- Molecular Structure: Figure 1 illustrates the molecular structure of $\mathbf{L_1}$-$\mathbf{L_5}$ as computed by DFT. For 3,8-diphenyl-1,10-phenanthroline ($\mathbf{L_1}$), the phenyl ring is twisted by 39.3°/39.3 ° with respect to the central *phen* core. These values closely align with the 40.0° measured by diffraction and previously reported values for 3,8-bis(4-methylphenyl)-1,10-phenanthroline, 25.7°/32.3° [34] and the coordinated ligand in (3,8-diphenyl-1,10-phenanthroline)-tris[1,1,1-trifluoro-4-(hy-droxy)-4-(thiophen-2-yl)but-3-en-2-onato]-europium(III) (33.5°/6.7°) [35]. The computed dihedral angles for $\mathbf{L_2}$, $\mathbf{L_3}$, $\mathbf{L_4}$ and $\mathbf{L_5}$ are 57.3°/58.5°, 37.8°/39.0°, 82.3°/82.3° and 55.5°/57.1° respectively. The results suggest that the twisting of both arms is unsymmetrical, and the more the number of carbon rings in the aromatic arms, the higher the twisting angle. Additionally, the differences between $\mathbf{L_2}$ and $\mathbf{L_3}$ suggest that a or b connections of the naphthyl ring also play a role. Notably, anthryl substitution over pyrenyl leads to the highest dihedral angles, resembling the behavior observed for β-naphthyl. Interestingly, steric hindrance with phenanthroline hydrogen atoms prevents free rotation of the phenyl rings around the carbon-carbon bond.

3.2.- Electronic Structure. Figure 2 displays the frontier and near frontier Kohn-Sham levels for of $\mathbf{L_1}$-$\mathbf{L_5}$ as computed by DFT for the optimized geometry. The results confirm that the HOMO-LUMO energy gap diminishes as the number of carbon rings in the arms increases. However, the connection mode of the arm also plays a role, as evidenced by the lower gap for the β-naphthyl (3.93 eV) isomer compared to the α-naphthyl (4.07 eV). Across the complete series of molecules, the HOMO and LUMO correspond to π and π* orbitals.

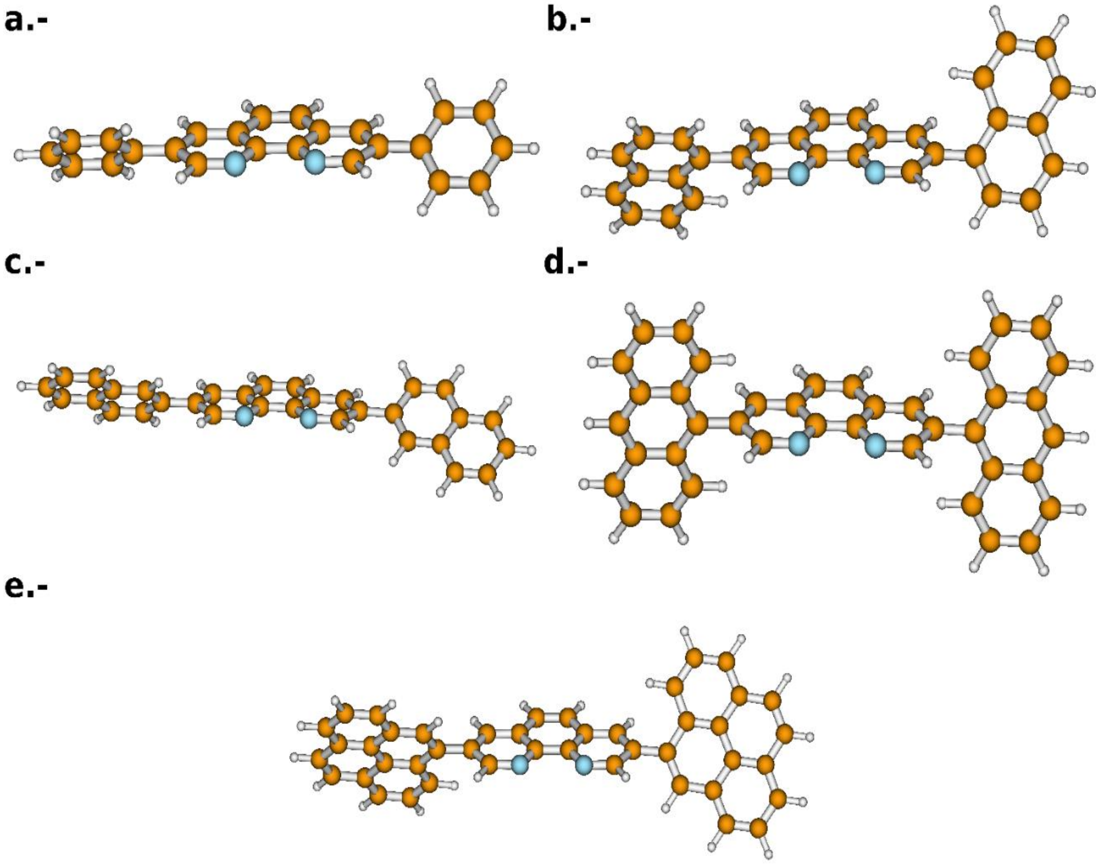

Figure 1. Molecular structure of $\mathbf{L_1}$-$\mathbf{L_5}$ as computed by DFT.

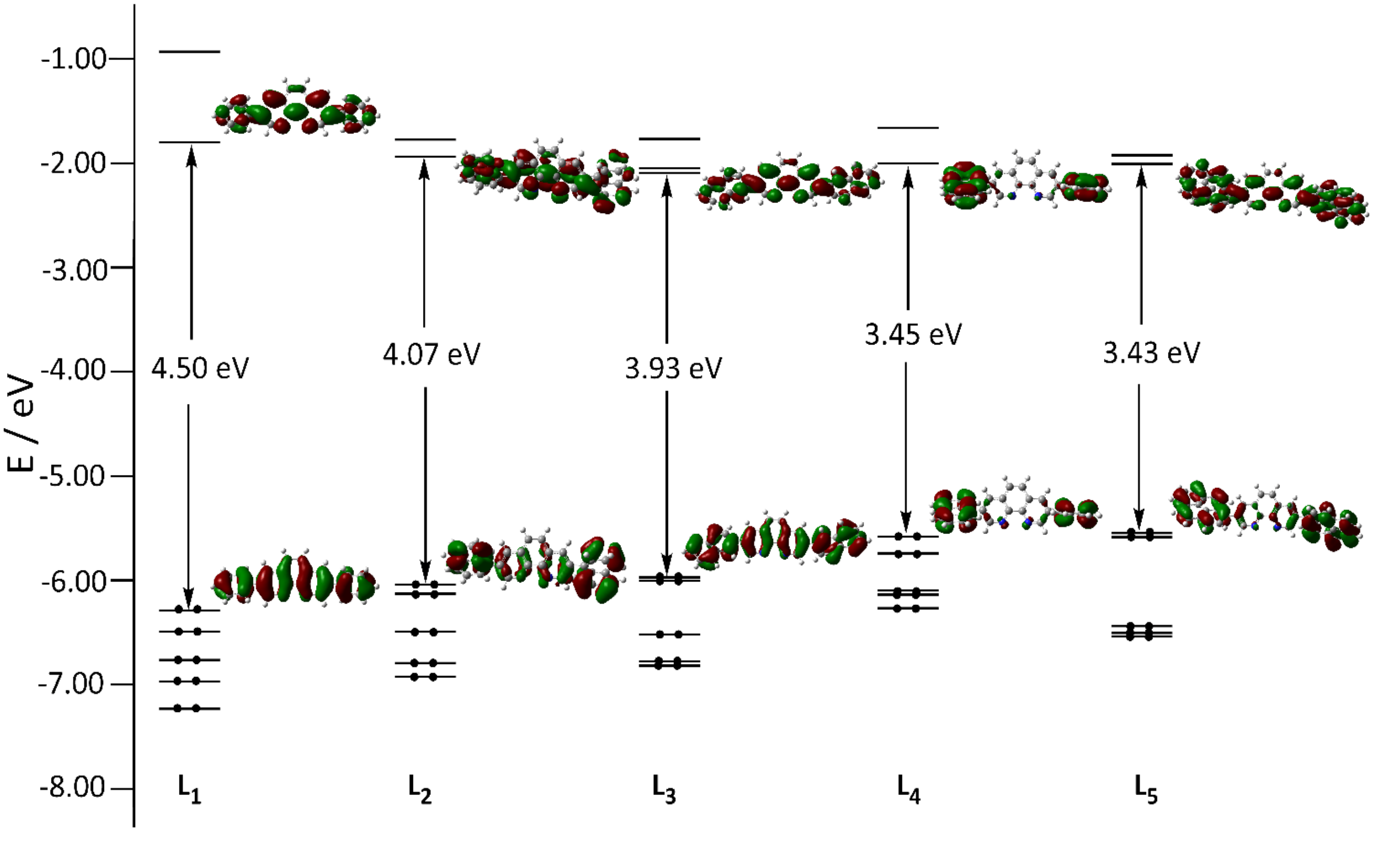

Figure 2. Frontier and near frontier Kohn-Sham levels for of $\mathbf{L_1}$-$\mathbf{L_5}$ as computed by DFT.

Notably, for **L_1**-**L_3**, they involved the entire molecule, including the central *phen* core and the aryl arms. In contrast, for **L_5**, the HOMO and LUMO are placed mostly on the aromatic arms, while for **L_4** they are placed almost exclusively on them. This structural variation significantly impacts the spectroscopic and electrochemical properties, as we will explore further in the corresponding sections.

3.3.- Electrochemical behavior: To characterize their electrochemical properties, voltammetric profiles at room temperature were measured for **L_1**-**L_5**.

The cyclic voltammograms (CVs) of **L_1**-**L_5** are shown in Figure 3. Ligands **L_1**, **L_4** and **L_5** exhibit two low intensity irreversible oxidation processes at potentials higher than 0.8 V. In contrast, in the reduction region, reversible processes occur, with half-wave potentials higher than -1.7 V, and irreversible processes at –1.07 V, -1.24 V and –1.28 V for **L_1**, **L_4** and **L_5**, respectively, attributed to reductions centered on the 1,10-phenanthroline core. The measured values for 1,10-phenanthroline in our system are -1.00 V; -1.25; -1.30 V, suggesting limited electronic mixing with the aromatic arms. Similar behavior has been noted in aromatic substituents of 1,10-phenanthroline which involve irreversible processes of the ligands and electrochemical decomposition products[36-38]. These electrochemical responses suggest that these chelating ligands could act as π-electron donors in organic metal complexes [39, 40]. For **L_2** and **L_3**, only non-reversible reduction processes are evident. An irreversible low intensity reduction process occurs at –1.14 V and –2.12 V for **L_2** and **L_3**, respectively, and low intensity non-reversible oxidation for **L_2**.

3.4.- Photophysical behavior:

The UV-Vis spectra of **L_1**-**L_5** in MeCN at room temperature are shown in Figure 4. The high-energy absorption bands at around 275 nm can be attributed to a pp* transitions involving the central *phen* core.

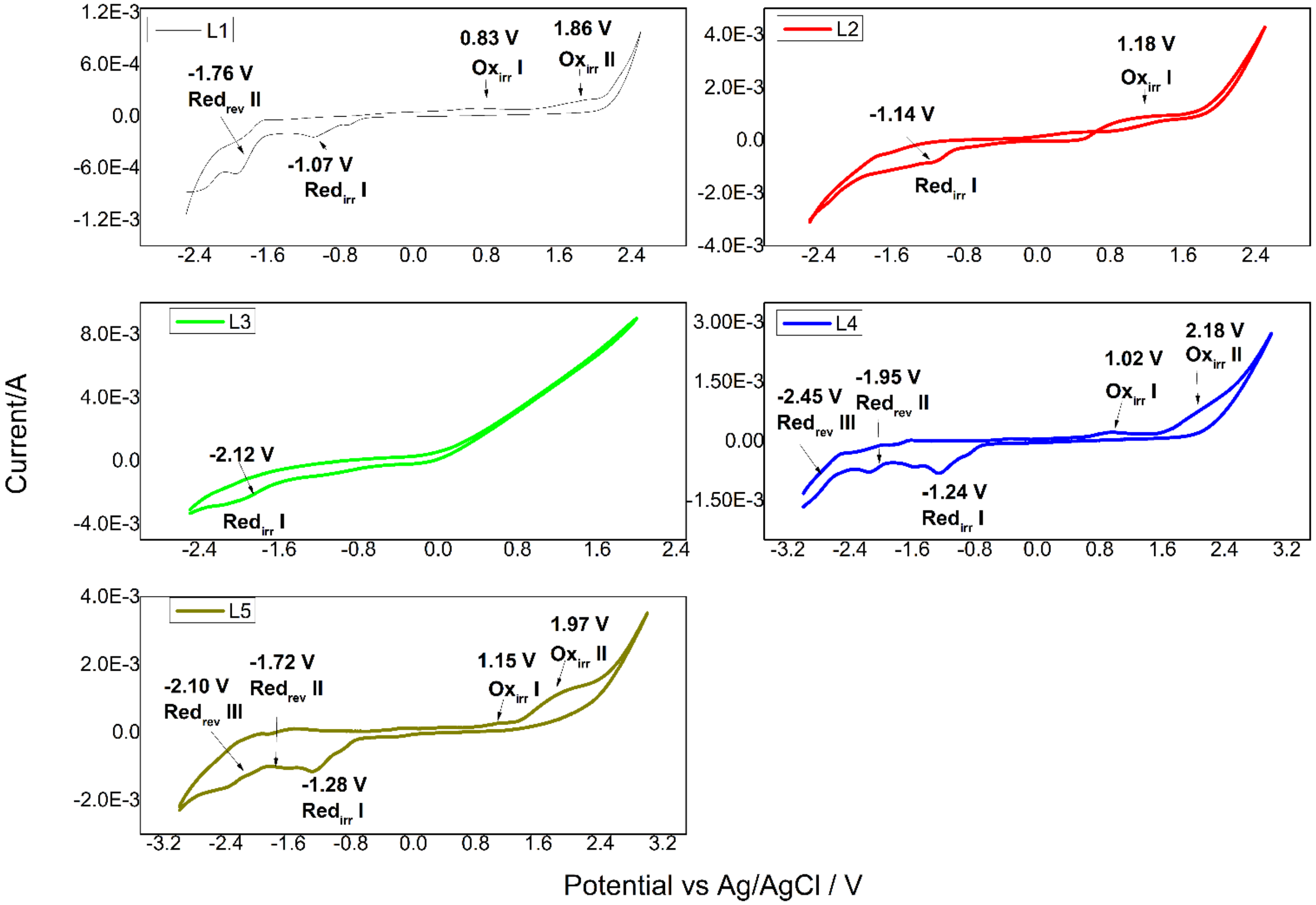

Figure 3. CVs of the ligand **L_1**-**L_5**. Interface: FTO| 2 x 10^{-3} mol L^{-1} of respective ligand + 10^{-1} mol L^{-1} of $TBAPF_6$ in DMF under an argon atmosphere. Scan rate: 100 mV s^{-1}.

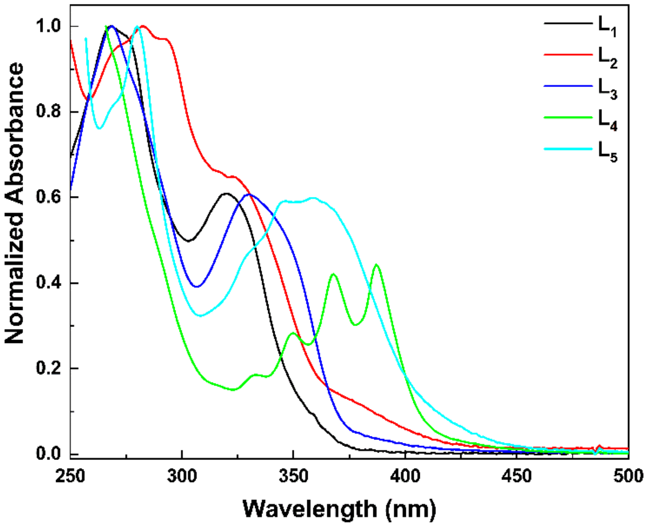

Figure 4. UV−Vis absorption spectra of L_1-L_5 in acetonitrile (MeCN) solution at room temperature.

In contrast, the low-energy absorption bands are assigned to a pp* transition with contributions of the entire molecule for L_1-L_3, consistent with the computed DFT results. The bathochromic shift of the low-energy absorption bands in L_4 and L_5 can be explained by pp* transitions centered on the anthryl and pyrenyl substituents. Similar behavior has been previously reported by Machura *et al* [41] for aryl-substituted terpyridines, where a higher contribution in the transitions was found for the more voluminous polyaromatic substituents.

Table 1 show a summary of the main photophysical data measured for L_1-L_5. As the date show, the absorption maxima and molar extinction coefficients do not show any significant solvatochromic effect for each molecule.

Figure 5 displays the emission spectra of L_1-L_5 in acetonitrile at room temperature upon excitation at their low-energy maxima absorption bands. Notably, the emission is centered between 380 nm to 400 nm for L_1-L_3. However, for L_4 and L_5, the maxima are significatively red-shifted to 450 nm and 460 nm, respectively.

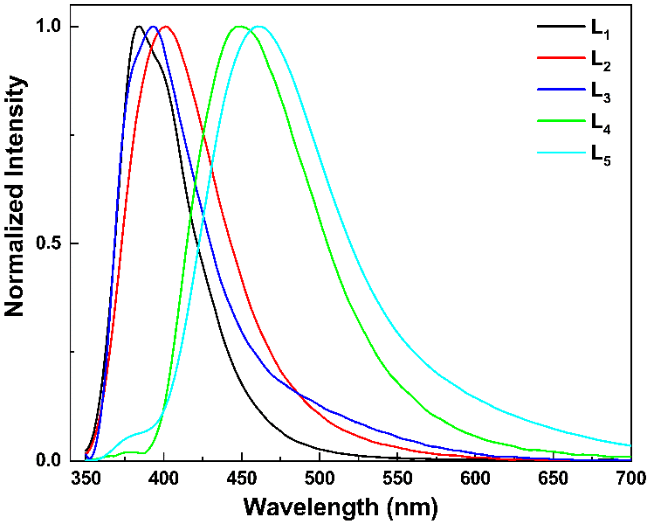

Figure 5. Emission spectra of L_1-L_5 in acetonitrile (MeCN) solution at room temperature. l_{exc} = 340 nm or 350 nm.

Furthermore, in contrast to L_1-L_3, the emission maxima for L_4 and L_5 are sensitive to the solvent polarity as clear from Table 2. An increase in polarity results in a bathochromic displacement of the emission. This behavior can be attributed to excited states with higher charge transfer character for L_4 and L_5, compared to L_1-L_3.

Table 1. Summary of the main photophysical properties of L_1-L_5 in MeCN or DCM at 298 K and in **EtOH:MeOH** (4:1) at 77 K.[a]

Compound	Solvent	λ_{abs} / nm (ε / 10^4 M^{-1} cm^{-1})	λ_{em} / nm	$\Phi_{em,air}$	$\Phi_{em,Ar}$	$\tau_{em,air}$ / $ns^{c,d}$ (%)	$\tau_{em,77K}$ / $ns^{c,d}$ (%)	Φ_Δ^d
L_1	DCM	273 (3.40), 320 (2.40)	407	0.12	0.15	1.20 (43), 3.70 (57)	-	0.30
	MeCN	270 (3.50), 320 (2.30)	384	0.05	0.07	1.69 (82), 3.78 (18)	-	-
	EtOH:MeOH	-	385	-	-	1.58 (43), 4.06 (57)	1.70 (92), 8.35 (8)	-
L_2	DCM	282 (3.10), 330 (2.20)	392	0.17	0.20	1.36 (98), 3.90 (2)	-	0.27
	MeCN	282 (2.45), 324 (1.70)	401	0.23	0.24	1.30 (29), 5.45 (71)	-	0.47
	EtOH:MeOH	-	410	-	-	1.47 (62), 1.59 (38)	1.38 (94), 2.66 (6)	-
L_3	DCM	270 (7.10), 330 (4.25)	396	0.35	0.40	1.41 (68), 2.16 (32)	-	0.18
	MeCN	270 (6.40), 330 (3.90)	393	0.36	0.41	1.65 (60), 2.24 (40)	-	0.45
	EtOH:MeOH	-	405	-	-	1.84 (99), 12.8 (1)	1.51 (89), 4.40 (11)	-
L_4	DCM	256 (18.4), 389 (2.14)	430	0.21	0.23	1.86	-	0.27
	MeCN	253 (18.7), 387 (2.19)	450	0.17	0.19	1.93	-	0.46
	EtOH:MeOH	-	470	-	-	1.13	2.35	-
L_5	DCM	282 (6.76), 360 (4.40)	445	0.32	0.39	1.65	-	0.12
	MeCN	280 (6.57), 360 (4.37)	460	0.50	0.52	2.08	-	0.12
	EtOH:MeOH	-	475	-	-	1.75	1.51	-

[a] Errors were lower than 10%. [b] λ_{ex} = 340 nm. [c] χ^2 parameters were between 0.998 and 1.066. [d] λ_{ex} = 355 nm.

The emission quantum yield values (F_{em}) exhibit in Table 1 are ranged between 0.17 to 0.52 for L_2-L_5, while L_1 has the lowest values. This parameter was slightly sensible to the oxygen presence in the media, consistent with excited states with singlet character.

Time-resolved emission experiments allow to get fluorescence lifetimes for L_1-L_5 in MeCN and DCM at room temperature (Figure S16), and in EtOH:MeOH (4:1) glass matrix at 77 K.

The emission decays for L_1-L_3 exhibit good fits to biexponential decays with two lifetimes in the order of the nanoseconds, whereas monoexponential emission decays are obtained for L_4 and L_5. A plausible explanation for these differing behaviours is that while HOMO and LUMO orbitals for L_1-L_3 encompass the entire molecules, resulting in significant contributions from π-π^* transitions, a partial charge transfer transition is also possible. In contrast, for L_4-L_5, a singlet excited state with charge transfer character appears to be the sole deactivation pathway. Interestingly, a similar behavior is observed at low temperatures (77 K).

The emission spectra observed at 77 K in Figure 6 exhibit similar features for L_2-L_3, characterized by structuration and maximum at 390 nm, along with a shoulder at 410 nm. In contrast, L_4-L_5 display maxima around 412 nm, accompanied by shoulders at 430 nm and 465 nm.

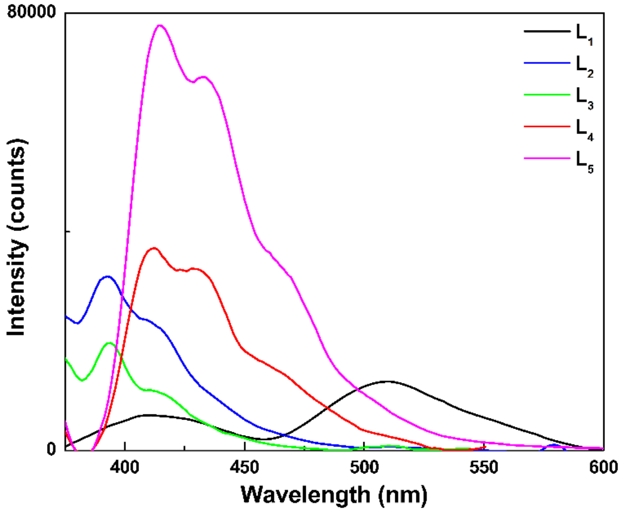

Figure 6. Emission spectra of **L_1-L_5** in EtOH:MeOH (4:1) glass matrix at 77 K. l_{exc} = 355 nm.

The emission spectrum of **L_1** exhibits maxima at 410 nm and 510 nm, which can be explained in terms of the formation π-stacked exciplex species in constrained media. Interestingly, this phenomenon occurs even at the low concentrations essayed and is completely absent for the other members of the series, suggesting blocking by their larger arms.

The complete series of compounds **L_1-L_5** can sensitize molecular oxygen in solution upon excitation at 355 nm, with relatively high singlet oxygen generation quantum yields (F_D), as shown in Table 1. This behavior is consistent with a significant evolution of the former singlet excited state produced upon excitation of **L_1-L_5** towards a triplet excited state. The possibility of a locally excited state exclusively centered on the polyaromatic arms can be ruled out due to the higher reported values of F_D for naphthalene, anthracene and pyrene.[42]

CONCLUSIONS

A series of 3,8-disubstituted 1,10-phenanthroline molecules with variable polyaromatic arms—namely, 3,8-diphenyl-1,10-phenanthroline (**L_1**), 3,8-di(naphthalen-1-yl)-1,10-phenanthroline (**L_2**), 3,8-di(naphthalen-2-yl)-1,10-phenanthroline (**L_3**), 3,8-di(anthracen-9-yl)-1,10-phenanthroline (**L_4**) and 3,8-di(pyren-1-yl)-1,10-phenanthroline (**L_5**) — can be efficiently prepared with good yields by coupling 3,8-dibromo-1,10-phenanthroline with a boronic acid catalyzed by [$Pd(PPh_3)_4$]. The results reveal that the electronic structure and the HOMO-LUMO gap primarily depend on the number, size and connection mode of the fused aromatic rings bonded to the phenanthroline central core, as reflected by their redox and photophysical properties. The absorption and emission properties are influenced by the degree of electronic interaction between the polyaromatic substituents and the phenanthroline core. Additionally, this interaction leads to different emissive ππ* excited states for the molecules bearing the most voluminous anthryl and pyrenyl substituents, conferring them a more charge transfer character, and greater sensitivity to solvent polarity. The photosensitizing capacity of singlet oxygen generation upon excitation of **L_1-L_5** in solution is consistent with a significant evolution of the former singlet excited state towards a triplet excited state. The combination of these rich properties makes these molecules a valuable set for the preparation of metal complexes with predictable properties.

SUPPORTING INFORMATION

NMR, IR, HRMS and additional spectroscopic data tables and images.

ACKNOWLEDGEMENTS

The authors acknowledge financial support from National Agency for Research and Development (ANID) through grants 1200418 (A.V.), 1200903 (N.P) and 3210010 (J.M) and Millennium Institute on Green Ammonia as Energy Vector MIGA (ANID/Millennium Science Initiative Program) ICN2021_023 (R.A). AV also acknowledges the support of Financiamiento Basal AFB220001 Project (CEDENNA).

REFERENCES

1. Pashaei, B., et al., *Polypyridyl ligands as a versatile platform for solid-state light-emitting devices.* Chemical Society Reviews, 2019. **48** (19): p. 5033-5139.
2. Yip, A.M.-H. and K.K.-W. Lo, *Luminescent rhenium(I), ruthenium(II), and iridium(III) polypyridine complexes containing a poly(ethylene glycol) pendant or bioorthogonal reaction group as biological probes and photocytotoxic agents.* Coordination Chemistry Reviews, 2018. **361**: p. 138-163.
3. Martínez-Alonso, M. and G. Gasser, *Ruthenium polypyridyl complex-containing bioconjugates.* Coordination Chemistry Reviews, 2021. **434**: p. 213736.
4. Adeloye, A.O. and P.A. Ajibade, *Towards the Development of Functionalized PolypyridineLigands for Ru(II) Complexes as Photosensitizers inDye-Sensitized Solar Cells (DSSCs).* Molecules, 2014. **19**(8): p. 12421-12460.
5. Choroba, K., et al., *Aryl substituted 2,6-di(thiazol-2-yl)pyridines –excited-state characterization and potential for OLEDs.* Dyes and Pigments, 2019. **169**: p. 89-104.
6. Sravani Gudikandula, A.K., Navaneetha Nambigari, *Application of Ru(II) polypyridyl complexes in metallopharmaceuticals and material science.* Mediterranean Journal of Chemistry, 2023. **13**(3): p. 263-284.
7. Schramm, F., et al., *Expanding the Coordination Cage: A Ruthenium(II)−Polypyridine Complex Exhibiting High Quantum Yields under Ambient Conditions.* Inorganic Chemistry, 2009. **48**(13): p. 5677-5684.
8. Campagna, S., et al., *Photochemistry and Photophysics of Coordination Compounds: Ruthenium*, in *Photochemistry and Photophysics of Coordination Compounds I*, V. Balzani and S. Campagna, Editors. 2007, Springer Berlin Heidelberg: Berlin, Heidelberg. p. 117-214.
9. Louërat, F. and P.C. Gros, *Functional polypyridine ligands from copper-mediated room temperature coupling of 4-chloro-2-trimethylsilylpyridine.* Tetrahedron Letters, 2010. **51**(27): p. 3558-3560.
10. Ferreira, H., M.M. Conradie, and J. Conradie, *Cyclic voltammetry data of polypyridine ligands and Co(II)-polypyridine complexes.* Data in Brief, 2019. **22**: p. 436-445.
11. Sammes, P.G. and G. Yahioglu, *1,10-Phenanthroline: a versatile ligand.* Chemical Society Reviews, 1994. **23**(5): p. 327-334.
12. Bencini, A. and V. Lippolis, *1,10-Phenanthroline: A versatile building block for the construction of ligands for various purposes.* Coordination Chemistry Reviews, 2010. **254**(17): p. 2096-2180.
13. Kulapina, E.G. and N.M. Makarova, *Potentiometric Sensors Based on Various Active Components for the Multisensor Determination of Anionic and Nonionic Surfactants.* Journal of Analytical Chemistry, 2022. **77**(2): p. 173-184.
14. Estalayo-Adrián, S., et al., *Effect of Alkyl Chain Length on the Photophysical, Photochemical, and Photobiological Properties of Ruthenium(II) Polypyridyl Complexes for Their Application as DNA-Targeting, Cellular-Imaging, and Light-Activated Therapeutic Agents.* ACS Applied Bio Materials, 2021. **4**(9): p. 6664-6681.
15. Uflyand, I.E. and G.I. Dzhardimalieva, *Molecular design of supramolecular polymers with chelated units and their application as functional materials.* Journal of Coordination Chemistry, 2018. **71**(9): p. 1272-1356.
16. Ding, X., H. Xie, and Y.J. Kang, *The significance of copper chelators in clinical and experimental application.* The Journal of Nutritional Biochemistry, 2011. **22**(4): p. 301-310.
17. Duce, J.A. and A.I. Bush, *Biological metals and Alzheimer's disease: Implications for therapeutics and diagnostics.* Progress in Neurobiology, 2010. **92**(1): p. 1-18.
18. S. Ressalan and C.S.P. Iyer, *Review of Spectrofluorimetric Methods for the Determination of Copper, Nickel and Zinc.* Reviews in Analytical Chemistry, 2004. **23**(3): p. 159-232.
19. Case, F.H. and R. Sasin, *Substituted 1,10-phenanthrolines. VIII. 2- and 3-phenyl derivatives.* The Journal of Organic Chemistry, 1955. **20**(10): p. 1330-1336.
20. Li, B., et al., *Direct arylation of phenanthroline derivatives via oxidative C–H/C–H cross-coupling: synthesis and discovery of excellent ligands.* Organic & Biomolecular Chemistry, 2013. **11**(8): p. 1290-1293.
21. Li, X., et al., *Synthesis and characterization of novel rhenium(I) complexes with large Stokes shift for applications in organic electroluminescent devices.* Journal of Photochemistry and Photobiology A: Chemistry, 2012. **241**: p. 1-7.

22. Ritter, K., et al., *Optimized synthesis of a tert-butyl-phenyl-substituted tetrapyridophenazine ligand and its Ru(II) complexes and determination of dimerization behaviour of the complexes through supramolecular "Fingerhakel"*. Dalton Transactions, 2015. **44**(19): p. 8889-8905.
23. Nishikawa, Y. and H. Yamamoto, *Iron-Catalyzed Asymmetric Epoxidation of β,β-Disubstituted Enones.* Journal of the American Chemical Society, 2011. **133**(22): p. 8432-8435.
24. Rothe, C., et al., *Ionic Iridium(III) Complexes with Bulky Side Groups for Use in Light Emitting Cells: Reduction of Concentration Quenching.* Advanced Functional Materials, 2009. **19**(13): p. 2038-2044.
25. Crosby, G.A. and J.N. Demas, *Measurement of photoluminescence quantum yields. Review.* The Journal of Physical Chemistry, 1971. **75**(8): p. 991-1024.
26. Suzuki, K., et al., *Reevaluation of absolute luminescence quantum yields of standard solutions using a spectrometer with an integrating sphere and a back-thinned CCD detector.* Phys Chem Chem Phys, 2009. **11**(42): p. 9850-60.
27. Lakowicz, J.R., *Principles of fluorescence spectroscopy*. 2006, New York: Springer.
28. Schmidt, R., et al., *Phenalenone, a universal reference compound for the determination of quantum yields of singlet oxygen $O_2(^1\Delta_g)$ sensitization.* Journal of Photochemistry and Photobiology A: Chemistry, 1994. **79**(1-2): p. 11-17.
29. Frisch, M.J.T., G. W.; Schlegel, H. B.; Scuseria, G. E.; Robb, M. A.; Cheeseman, J. R.; Scalmani, G.; Barone, V.; Mennucci, B.; Petersson, G. A.; Nakatsuji, H.; Caricato et al., *Gaussian 09*. 2009, Gaussian, Inc.: Wallingford CT.
30. Miertuš, S., E. Scrocco, and J. Tomasi, *Electrostatic interaction of a solute with a continuum. A direct utilizaion of AB initio molecular potentials for the prevision of solvent effects.* Chemical Physics, 1981. **55**(1): p. 117-129.
31. Miertuš, S. and J. Tomasi, *Approximate evaluations of the electrostatic free energy and internal energy changes in solution processes.* Chemical Physics, 1982. **65**(2): p. 239-245.
32. Sheppard, C.L., et al., *Polynuclear copper(II) complexes with μ_2-1,1-azide bridges. Structural and magnetic properties.* Inorganica Chimica Acta, 1996. **250**(1-2): p. 227-239.
33. Humphrey, W., A. Dalke, and K. Schulten, *VMD: visual molecular dynamics.* J Mol Graph, 1996. **14**(1): p. 33-8, 27-8.
34. U. Florke, Y.V., M. Bauer., *3,8-bis(4-methylphenyl)-1,10-phenanthroline chloroform solvate.* CSD Communication(Private Communication), 2018.
35. Wang, X., et al., *Europium(III) complex fluorescent sensor for dual channel recognition of Sn^{2+} and Cu^{2+} ions in water.* Spectrochimica Acta Part A: Molecular and Biomolecular Spectroscopy, 2021. **250**: p. 119373.
36. Doettinger, F., et al., *Bichromophoric Photosensitizers: How and Where to Attach Pyrene Moieties to Phenanthroline to Generate Copper(I) Complexes.* Inorganic Chemistry, 2023. **62**(21): p. 8166-8178.
37. Benazzi, E., et al., *Bis(1,10-phenanthroline) copper complexes with tailored molecular architecture: from electrochemical features to application as redox mediators in dye-sensitized solar cells.* Electrochimica Acta, 2018. **271**: p. 180-189.
38. Wantulok, J., et al., *The effects of 4,7-di(pyrrolidin-1-yl) substituents on the reduction and oxidation mechanisms of 1,10-phenanthrolines: New perspectives in tailoring of phenantroline derivatives.* Electrochimica Acta, 2021. **370**: p. 137674.
39. Chen, C., et al., *Intramolecular Charge Transfer Controls Switching Between Room Temperature Phosphorescence and Thermally Activated Delayed Fluorescence.* Angewandte Chemie International Edition, 2018. **57**(50): p. 16407-16411.
40. Li, P., et al., *Intramolecular π Stacking in Cationic Iridium(III) Complexes with Phenyl-Functionalized Cyclometalated Ligands: Synthesis, Structure, Photophysical Properties, and Theoretical Studies.* European Journal of Inorganic Chemistry, 2014. **2014**(14): p. 2376-2382.
41. Szlapa-Kula, A., M. Małecka, and B. Machura, *Insight into structure-property relationships of aryl-substituted 2,2':6',2"-terpyridines.* Dyes and Pigments, 2020. **180**: p. 108480.
42. Wilkinson, F., W.P. Helman, and A.B. Ross, *Quantum Yields for the Photosensitized Formation of the Lowest Electronically Excited Singlet State of Molecular Oxygen in Solution.* Journal of Physical and Chemical Reference Data, 1993. **22**(1): p. 113-262.